AIMS Mathematics

https://www.aimspress.com/journal/Math

AIMS Mathematics, 11(8): 24282–24303.
DOI: 10.3934/math.2026980
Received: 03 June 2026
Revised: 20 July 2026
Accepted: 05 August 2026
Published: 10 August 2026

Research article

Global polynomial synchronization and stability of discrete-time inertial neural networks with proportional delays and its application to image encryption

Fengzhao Wang[1], **Xingjian chen**[1], **Cheng Yang**[1,2] **and Xuan Chen**[1,*]

[1] School of Physics and Electronic Science, Guizhou Normal University, Guiyang 550025, China
[2] Key Laboratory of Automotive Electronics Technology of Guizhou Provincial Department of Education, Guiyang 550025, China

* **Correspondence:** Email: cxgzsd@163.com.

Abstract: This paper investigates global polynomial synchronization (GPS) of discrete-time inertial neural networks with proportional delays (PD-DTINNs). A discrete-time model is formulated on the sampling grid $\hbar k$, where the proportional-delay state is directly represented by $x_j(\lfloor \mathfrak{p}_j k \rfloor \hbar)$, thereby avoiding the continuous-time logarithmic transformation commonly used for proportional delays. A simple feedback controller is designed for the corresponding drive–response PD-DTINNs. By constructing appropriate auxiliary functions and combining difference relations with norm estimates, a direct analytical approach is developed without constructing Lyapunov functionals or employing the matrix-measure technique. Based on this approach, delay-dependent and delay-independent criteria are established to guarantee GPS, from which the corresponding global asymptotic synchronization (GAS) results are obtained. The developed framework is further extended to the stability analysis of a single discrete-time inertial neural network with proportional delays, thus yielding criteria for global polynomial stability and global asymptotic stability. Finally, one numerical example is provided to verify the proposed results, and the obtained synchronization behavior is applied to image encryption and decryption, thus illustrating its potential application in image security.

Keywords: discrete-time inertial neural networks; proportional delays; global polynomial synchronization; image encryption
Mathematics Subject Classification: 39A30, 93C43, 94A60

1. Introduction

In various scientific and engineering domains, neural network models are now indispensable tools to tackle complex problems. Their applications span associative memory [1], secure communication [2], and environmental science [3]. Different applications are usually associated with different dynamical requirements. For example, stability and convergence are fundamental to optimization and associative memory, while synchronization plays an important role in secure communication and image encryption. As these dynamical requirements become more refined, neural network models with richer structures have been developed. Babcock and Westervelt [4] proposed inertial neural networks (INNs) by augmenting traditional first-order networks with an inertial term, which represents an inductive effect. The second-order structure of INNs may induce complex phenomena such as oscillation, bifurcation, and chaos. This increased dynamical complexity has motivated extensive investigations into the synchronization of INNs. Specifically, global asymptotic synchronization (GAS) [5], exponential synchronization [6], finite-time synchronization [7], and fixed-time synchronization [8] have been established for different classes of INNs. However, most of these studies focus on continuous-time INNs, whereas synchronization of discrete-time INNs has been much less investigated. As pointed out in [9], in practical applications, most digital devices and numerical algorithms work in a discrete-time manner. Although continuous-time neural networks (NNs) can be discretized for implementation, the discretization process may change or even fail to preserve the original dynamical behavior of the continuous-time models. Therefore, it is meaningful to directly investigate INNs in the discrete-time framework.

Time delays are often encountered in NNs and may affect their dynamical behaviors. In existing NN models, constant delays [10], time-varying delays [11], distributed delays [12], leakage delays [13], and mixed delays [14] have been widely considered. Among various types of delays, the proportional delay is a special time-dependent delay, where the delayed argument is proportional to the current time. It is usually described by $x_i(qt), 0 < q < 1$, where $qt = t - (1 - q)t$ and $\tau(t) = (1 - q)t$ denotes the corresponding delay function. Since $\tau(t) \to \infty$ as $t \to \infty$, proportional delays are essentially different from constant delays and bounded time-varying delays. For continuous-time systems, a common way to handle such delays is to use the logarithmic transformation $y_i(s) = x_i(e^s)$, under which

$$x_i(qt) = x_i(qe^s) = x_i(e^{s+\ln q}) = y_i(s + \ln q) = y_i\left(s - \tau_q\right), \tau_q = -\ln q > 0.$$

Therefore, the proportional delay term can be converted into a constant delay term τ_q. Based on this idea, many studies have transformed proportional-delay NNs into equivalent NNs with constant delays and time-varying coefficients, and then analyzed their dynamical properties using Lyapunov functionals, differential inequalities, or matrix methods. For example, Zhou first investigated the global asymptotic stability of cellular NNs with a single proportional delay [15] and later studied the global exponential dissipativity of impulsive NNs with multiple proportional delays via Lyapunov functionals and matrix norm methods [16].

Owing to the unbounded nature of proportional delays, the convergence behavior of proportional-delay systems may not always be adequately characterized by exponential estimates, and imposing exponential decay may sometimes be overly restrictive. Against this background, global polynomial synchronization (GPS), originating from the concept of polynomial stability [17], has recently attracted increasing attention. The concept of GPS was introduced by Zhou and Zhao [18] in the study of recurrent NNs with proportional delays, where the synchronization error was characterized by an explicit algebraic decay rate. Unlike GAS, which merely guarantees that the synchronization error eventually converges to zero, GPS provides quantitative information on the convergence behavior. Although polynomial convergence is generally slower than exponential convergence, it offers a meaningful complementary framework for systems whose decay behavior cannot be effectively described by exponential bounds. Recently, Wan et al. [19] investigated GPS for parameter-uncertain memristive NNs with proportional delays. Guo and Zhou [20] further extended the analysis to a complex-valued memristive NNs incorporating spatial diffusion and fuzzy dynamics, and derived GPS criteria under an adaptive event-triggered scheme. Zhang et al. [21] extended the GPS analysis to a quaternion-valued INNs incorporating fuzzy rules and polynomial gains. Nevertheless, these results were developed for continuous-time systems, and GPS of discrete-time INNs with proportional delays (PD-DTINNs) has not been fully investigated.

Motivated by the above discussions, this paper investigates the GPS problem for a class of PD-DTINNs. Different from continuous-time approaches based on logarithmic transformations, the proportional delay terms are directly handled in the discrete-time framework. To handle the inertial dynamics of the considered network, the drive-response PD-DTINNs are constructed, and the reduced-order method is applied to transform the synchronization error system into an equivalent first-order form. Instead of constructing Lyapunov functionals or using matrix-measure methods, the difference definition, auxiliary functions, and properties of matrix and vector norms are employed to analyze the system. As a result, some delay-dependent and delay-independent criteria are derived to guarantee GPS. Finally, the obtained theoretical results are applied to image encryption, which illustrates their effectiveness and potential application value.

The main contributions are summarized as follows:

(i) A discrete-time inertial neural network with proportional delays is formulated on the sampling grid $\hbar k$, where the delayed state is directly represented by $x_j(\lfloor \mathrm{p}_j k \rfloor \hbar)$. This work addresses the relatively unexplored problem of GPS for proportional-delay INNs directly formulated in a discrete-time framework.

(ii) A direct analytical approach is developed by combining auxiliary-function construction, difference relations, and norm estimates, without constructing Lyapunov functionals. Based on a simple feedback controller, delay-dependent and delay-independent criteria for GPS are established, together with the corresponding GAS results. The obtained conditions are concise and readily verifiable.

(iii) The proposed framework is further extended to the stability analysis of a single discrete-time proportional-delay INN, yielding criteria for global polynomial stability and global asymptotic stability. Moreover, the synchronization results are applied to image encryption and decryption, thus illustrating their potential value in image security.

Notations. Throughout this paper, $\mathbb{R}, \mathbb{Z}$ are the real number set and the integer set, respectively. $\mathcal{I}_n := \{1, 2, \cdots, n\}$. $\mathcal{J}_n := \{0, 1, 2, \cdots, n\}$. $\mathrm{diag}\{q_i\}_n$ denotes the diagonal matrix with its diagonal elements $q_1, q_2, \cdots, q_n$. I denotes the $n \times n$ identity matrix. For symmetrical matrix Q, $Q > 0$ means that Q is a positive definite matrix, and Q^2 represents $Q \times Q$. For symmetric matrices $Q_1, Q_2, Q_1 \leq Q_2$ means $Q_1 - Q_2$ is a semidefinite matrix, $\|\mathrm{O}\|_p$ denotes the p norm of matrix O, $\lfloor \cdot \rfloor$ denotes the floor function, the greatest integer less than or equal to its argument. $\ell_{min}(Q)$ denote the minimum eigenvalues of Q.

2. Preliminaries and model description

Consider the following PD-DTINNs:

$$\Delta_{\hbar}^{2}x_i(\hbar k) = -a_i^*\Delta_{\hbar}x_i(\hbar k) - b_i^*x_i(\hbar k) + \sum_{j=1}^{n} c_{ij}^* g_j(x_j(\hbar k)) + \sum_{j=1}^{n} d_{ij}^* g_j(x_j(\lfloor \mathfrak{p}_j k\rfloor \hbar)) + R_i, \quad k \geq k_0, \tag{2.1}$$

where n is the number of neurons, $i, j \in \mathcal{I}_n$, $k \in \mathcal{J}_n$, $\hbar > 0$ is the sampling step size, $x_i(\hbar k) \in \mathbb{R}$ is the state of the ith neuron at time $\hbar k$, and $\hbar k_0$ is the initial instant of System (2.1). $\Delta_{\hbar}x_i(\hbar k)$ and $\Delta_{\hbar}^2 x_i(\hbar k)$ denote the forward difference and inertial term of PD-DTINNs (2.1), respectively, and are defined as follows:

$$\begin{cases} \Delta_{\hbar}x_i(\hbar k) = \dfrac{x_i(\hbar(k+1)) - x_i(\hbar k)}{\hbar}, \\ \Delta_{\hbar}^2 x_i(\hbar k) = \dfrac{\Delta_{\hbar}x_i(\hbar(k+1)) - \Delta_{\hbar}x_i(\hbar k)}{\hbar}, \end{cases} \tag{2.2}$$

c_{ij}^* and d_{ij}^* represent the connection weights, $a_i^* > 0$ and $b_i^* > 0$ are self-feedback coefficients, $g_j(\cdot)$ is the activation function, and R_i is the external input. $\mathfrak{p}_j \in (0, 1]$ is the proportional delay factor with $\tilde{\mathfrak{p}} = \min_{\mathcal{I}_n}\{\mathfrak{p}_j\}$. Here, $\lfloor \mathfrak{p}_j k\rfloor \hbar$ denotes the proportional delay term, in which $\lfloor \mathfrak{p}_j k\rfloor$ is the greatest integer less than or equal to $\mathfrak{p}_j k$.

With the initial conditions,

$$\begin{cases} x_i(\sigma\hbar) = \varphi_{i\sigma}, \quad \sigma \in [\lfloor \tilde{\mathfrak{p}} k_0\rfloor, k_0 + 1]_{\mathbb{Z}}, \\ \Delta_{\hbar}x_i(\sigma\hbar) = \dfrac{\varphi_i(\sigma + 1) - \varphi_i(\sigma)}{\hbar} \triangleq \phi_{i\sigma}, \quad \sigma \in [\lfloor \tilde{\mathfrak{p}} k_0\rfloor, k_0]_{\mathbb{Z}}. \end{cases}$$

Remark 1. *In the proposed Model (2.1), the step size $\hbar > 0$ is introduced to describe the actual sampling time scale. Compared with discrete-time INNs usually defined only at integer instants [9,22], the introduction of $\hbar$ makes the model more consistent with the implementation of practical sampled-data systems.*

Remark 2. *The delay term $\lfloor \mathfrak{p}_j k\rfloor \hbar$ is called a proportional delay, where $0 < \mathfrak{p}_j \leq 1$ is the proportional delay factor. The term means that, at the current step k, the state of the jth neuron is evaluated at the proportional historical instant $\lfloor \mathfrak{p}_j k\rfloor \hbar$. Moreover, when $\mathfrak{p}_j < 1$, the corresponding delay step number can be written as $\tau_j(k) = k - \lfloor \mathfrak{p}_j k\rfloor$, and the actual delay length is $\tau_j(k)\hbar$, which is a time-varying and unbounded delay. This construction is motivated by the proportional delays in continuous-time NNs [15, 16, 19–21, 23], where $\mathfrak{p}_j t = t - (1 - \mathfrak{p}_j)t$ and $(1 - \mathfrak{p}_j)t$ is an unbounded delay function.*

Let

$$x(\hbar k) = (x_1(\hbar k), \ \ x_2(\hbar k), \ \ \cdots, \ \ x_n(\hbar k))^T,$$

$$g(x(\hbar k)) = (g_1(x_1(\hbar k)), \ \ g_2(x_2(\hbar k)), \ \ \cdots, \ \ g_n(x_n(\hbar k)))^T,$$

$$g(x(\lfloor \mathfrak{p} k\rfloor \hbar)) = (g_1(x_1(\lfloor \mathfrak{p}_1 k\rfloor \hbar)), \ \ g_2(x_2(\lfloor \mathfrak{p}_2 k\rfloor \hbar)), \ \ \cdots, \ \ g_n(x_n(\lfloor \mathfrak{p}_n k\rfloor \hbar)))^T,$$

$A^* = \mathrm{diag}[a_i^*]_n$, $B^* = \mathrm{diag}[b_i^*]_n$, $C^* = [c_{ij}^*]_{n\times n}$, $D^* = [d_{ij}^*]_{n\times n}$, and $R^* = (R_1, R_2, \cdots, R_n)^T$. Then, the vector form of PD-DTINNs (2.1) can be written as follows:

$$\Delta_{\hbar}^2 x(\hbar k) = -A^*\Delta_{\hbar}x(\hbar k) - B^*x(\hbar k) + C^*g(x(\hbar k)) + D^*g(x(\lfloor \mathfrak{p} k\rfloor \hbar)) + R^*. \tag{2.3}$$

Here, PD-DTINNs (2.3) serves as the drive system, and its corresponding response system is given as follows:

$$\Delta_\hbar^2 \eta(\hbar k) = -A^* \Delta_\hbar \eta(\hbar k) - B^* \eta(\hbar k) + C^* g(\eta(\hbar k)) + D^* g(\eta(\lfloor \mathfrak{p} k \rfloor \hbar)) + R^* + \mathcal{K}(\hbar k), \tag{2.4}$$

where $\mathcal{K}(\hbar k)$ denotes the proportional- delay-dependent control input, which will be specified later.

Let $e(\hbar k) = \eta(\hbar k) - x(\hbar k)$, $g(e(\hbar k)) = g(\eta(\hbar k)) - g(x(\hbar k))$ and $g(e(\lfloor \mathfrak{p} k \rfloor \hbar)) = g(\eta(\lfloor \mathfrak{p} k \rfloor \hbar)) - g(x(\lfloor \mathfrak{p} k \rfloor \hbar))$. Then, the synchronization error system can be described as follows:

$$\Delta_\hbar^2 e(\hbar k) = -A^* \Delta_\hbar e(\hbar k) - B^* e(\hbar k) + C^* g(e(\hbar k)) + D^* g(e(\lfloor \mathfrak{p} k \rfloor \hbar)) + \mathcal{K}(\hbar k). \tag{2.5}$$

Then, introduce the variable $y(\hbar k) = \Delta_\hbar e(\hbar k) + \Xi e(\hbar k)$ with $\Xi > 0$ and design the following controller:

$$\mathcal{K}(\hbar k) = -\alpha e(\hbar k) - \beta y(\hbar k) - \zeta e(\lfloor \mathfrak{p} k \rfloor \hbar). \tag{2.6}$$

The error System (2.5) can be written as follows:

$$\begin{cases} \Delta_\hbar e(\hbar k) = -\Xi e(\hbar k) + y(\hbar k), \\ \Delta_\hbar y(\hbar k) = -A y(\hbar k) - B e(\hbar k) + C^* g(e(\hbar k)) + D^* g(e(\lfloor \mathfrak{p} k \rfloor \hbar)) - \zeta e(\lfloor \mathfrak{p} k \rfloor \hbar), \end{cases} \tag{2.7}$$

where $A = A^* - \Xi + \beta$, $B = -\Xi A^* + \Xi^2 + B^* + \alpha$.

Remark 3. *The state feedback controller (2.6) consists of three parts: the current synchronization error term $e(\hbar k)$, the auxiliary error term $y(\hbar k)$, and the proportional-delay synchronization error term $e(\lfloor \mathfrak{p} k \rfloor \hbar)$, with the corresponding control gains α, β, and ζ, respectively. Among them, $y(\hbar k)$ originates from the reduced-order method of INNs and reflects the first-order difference dynamics of the error system. The term $e(\lfloor \mathfrak{p} k \rfloor \hbar)$ can be regarded as a delay-error compensation. Compared with simple controllers which only involve the current error or the error difference [5, 24, 25], the proposed controller uses both the dynamic error information and the delayed error information, which helps improve the synchronization control performance. Moreover, the controller in this paper is directly imposed on the original response system, rather than on the transformed system [2, 6, 26]. This avoids the difficulty of restoring the transformed system with the controller to the original response system.*

Assumption 1. *The activation function $g_j(\cdot)$ is bounded and there exist holds for all $a, b \in \mathbb{R}$, $a \neq b$, $j \in \mathcal{I}_n$. Then,*

$$\left| g_j(a) - g_j(b) \right| \le \psi_j \left| a - b \right|,$$

where $\psi_j > 0$, and we denote $\Psi = \mathrm{diag}\{\psi_1, \psi_2, \ldots, \psi_n\}$.

Assumption 2. *Define the following:*

$$\begin{cases} \hat{\varphi} = \max\limits_{s \in [\lfloor \bar{\mathfrak{p}} k_0 \rfloor, k_0]_{\mathbb{Z}}} \{\|\bar{\varphi}(s\hbar) - \varphi(s\hbar)\|\}, \\ \hat{\phi} = \max\limits_{s \in [\lfloor \bar{\mathfrak{p}} k_0 \rfloor, k_0]_{\mathbb{Z}}} \{\|\bar{\phi}(s\hbar) - \phi(s\hbar)\|\}, \end{cases} \tag{2.8}$$

where $\bar{\varphi}(s\hbar)$, and $\bar{\phi}(s\hbar)$ is the initial value of the response System (2.4), either $\hat{\varphi}$ or $\hat{\phi}$ is positive. For example, if $\hat{\varphi} > 0$, then we can make $\hat{\phi} = 0$, i.e., $\bar{\phi}(s\hbar) = \phi(s\hbar)$. Since $\varphi((k_0 + 1)\hbar) = \varphi(k_0\hbar) + \hbar\phi(k_0\hbar)$, *we have* $\|\bar{\varphi}((k_0+1)\hbar) - \varphi((k_0+1)\hbar)\| \le \hat{\varphi} + \hbar\hat{\phi}$. *Therefore, the value at* $s = k_0 + 1$ *can be controlled by the above two initial bounds.*

Denote $\bar{\Phi} = \max\{\hat{\varphi}, \hat{\phi}\}$. *Since* $y(\hbar k) = \Delta_\hbar e(\hbar k) + \Xi e(\hbar k)$, *we obtain the following inequality:*

$$\max_{s\in[\lfloor\tilde{\mathfrak{p}}k_0\rfloor, k_0]_{\mathbb{Z}}} \|y(s\hbar)\| \le (\|I\| + \|\Xi\|)\bar{\Phi} \le \Phi \tag{2.9}$$

where $\Phi = \max\{\bar{\Phi}, (\|I\| + \|\Xi\|)\bar{\Phi}\}$.

Definition 1. *[19] The drive System (2.3) and response System (2.4) are said to be globally polynomially synchronized under the controller if there exist the positive constants* $\mathrm{M} > 0$ *and* $\lambda > 0$ *such that*

$$\|\eta(\hbar k) - x(\hbar k)\| \le \mathrm{M}\left[\frac{k+1}{k_0+1}\right]^{-\lambda}, \quad k \ge k_0 > \lfloor\tilde{\mathfrak{p}}k_0\rfloor, \tag{2.10}$$

where λ *is referred to as the polynomial synchronous decay rate, and* M *depends on the initial conditions* $\varphi_i(s\hbar), \phi_i(s\hbar)$, $\bar{\varphi}_i(s\hbar)$, *and* $\bar{\phi}_i(s\hbar), i \in \mathcal{I}_n$.

3. Main result

In this section, delay-dependent and delay-independent criteria are first derived to guarantee GPS of the drive-response PD-DTINNs. Then, the obtained results are extended to establish the global polynomial stability and global asymptotic stability criteria for a single PD-DTINN.

Theorem 1. *Suppose Assumptions 1 and 2 hold; for a given* $\Psi = \mathrm{diag}\{\psi_1, \psi_2, \ldots, \psi_n\}$, *the drive-response PD-DTINNs (2.3) and (2.4) achieve GPS under controller (2.6) with decay rate* λ *for some* $\lambda > 0$, *provided that*

$$\begin{cases} 1 < \ell_{min}(\Xi) < 1 + \dfrac{1}{\hbar}, \\ \ell_{min}(A) > \|B\| + \|C^*\| \cdot \|\Psi\| + \|D^*\| \cdot \|\Psi\| + \|\zeta\|. \end{cases} \tag{3.1}$$

Proof. It follows from (2.2) that the error System (2.7) can be described as follows:

$$\begin{cases} e(\hbar(k+1)) = (I - \hbar\Xi)e(\hbar k) + \hbar y(\hbar k), \\ y(\hbar(k+1)) = (I - \hbar A)y(\hbar k) - \hbar Be(\hbar k) + \hbar C^* g(e(\hbar k)) + \hbar D^* g(e(\lfloor\mathfrak{p}k\rfloor\hbar)) - \hbar\zeta \cdot e(\lfloor\mathfrak{p}k\rfloor\hbar). \end{cases} \tag{3.2}$$

By Assumption 1 and applying the 2−norm to both sides of (3.2) yield the following:

$$\begin{cases} \|e(\hbar(k+1))\| \le \|I - \hbar\Xi\|\|e(\hbar k)\| + \hbar\|y(\hbar k)\|, \\ \|y(\hbar(k+1))\| \le \|I - \hbar A\|\|y(\hbar k)\| + \hbar(\|B\| + \|C^*\| \cdot \|\Psi\|)\|e(\hbar k)\| \\ \qquad\qquad + \hbar(\|D^*\| \cdot \|\Psi\| + \|\zeta\|) \cdot \|e(\lfloor\mathfrak{p}k\rfloor\hbar)\|. \end{cases} \tag{3.3}$$

Note that $I - \hbar\Xi > 0$ and $I - \hbar A > 0$; if $\hbar$ is sufficiently small, then we have the following:

$$\begin{cases} \|I - \hbar\Xi\| = 1 - \hbar\ell_{min}(\Xi), \\ \|I - \hbar A\| = 1 - \hbar\ell_{min}(A). \end{cases} \tag{3.4}$$

Then, System (3.3) can be rewritten as follows:

$$\begin{cases} \|e(\hbar(k+1))\| \leq (1-\hbar\ell_{min}(\Xi))\|e(\hbar k)\| + \hbar\|y(\hbar k)\|, \\ \|y(\hbar(k+1))\| \leq (1-\hbar\ell_{min}(A))\|y(\hbar k)\| + \hbar(\|B\| + \|C^*\|\cdot\|\Psi\|)\|e(\hbar k)\| \\ \qquad\qquad + \hbar(\|D^*\|\cdot\|\Psi\| + \|\zeta\|)\cdot\|e(\lfloor \mathfrak{p}k\rfloor\hbar)\|. \end{cases} \tag{3.5}$$

For $\lambda > 0$, by multiplying both sides of (3.5) by $\left[\frac{k+2}{k_0+1}\right]^\lambda > 0$, we obtain the following:

$$\begin{cases} \|e(\hbar(k+1))\|\left(\dfrac{k+2}{k_0+1}\right)^\lambda \leq (1-\hbar\ell_{min}(\Xi))\|e(\hbar k)\|\left(\dfrac{k+2}{k_0+1}\right)^\lambda + \hbar\|y(\hbar k)\|\left(\dfrac{k+2}{k_0+1}\right)^\lambda, \\ \|y(\hbar(k+1))\|\left(\dfrac{k+2}{k_0+1}\right)^\lambda \leq (1-\hbar\ell_{min}(A))\|y(\hbar k)\|\left(\dfrac{k+2}{k_0+1}\right)^\lambda \\ \qquad\qquad + \hbar(\|B\| + \|C^*\|\|\|\Psi\|)\|e(\hbar k)\|\left(\dfrac{k+2}{k_0+1}\right)^\lambda \\ \qquad\qquad + \hbar(\|D^*\|\cdot\|\Psi\| + \|\zeta\|)\cdot\|e(\lfloor \mathfrak{p}k\rfloor\hbar)\|\left(\dfrac{k+2}{k_0+1}\right)^\lambda. \end{cases} \tag{3.6}$$

Define two auxiliary functions as follows:

$$\begin{cases} Q(\hbar k) = \|e(\hbar k)\|\left(\dfrac{k+1}{k_0+1}\right)^\lambda, \\ R(\hbar k) = \|y(\hbar k)\|\left(\dfrac{k+1}{k_0+1}\right)^\lambda, \end{cases} \qquad k \in [\lfloor \tilde{\mathfrak{p}}k_0\rfloor, +\infty)_{\mathbb{Z}}. \tag{3.7}$$

For any $k_0 \leq k$, $\frac{k+2}{k+1} \leq \frac{k_0+2}{k_0+1}$ holds, and we have

$$\left(\frac{k+2}{k_0+1}\right)^\lambda = \left(\frac{k+2}{k+1}\right)^\lambda \times \left(\frac{k+1}{k_0+1}\right)^\lambda \leq \mathcal{N}(\lambda)\left(\frac{k+1}{k_0+1}\right)^\lambda, \tag{3.8}$$

where

$$\mathcal{N}(\lambda) = \left(\frac{k_0+2}{k_0+1}\right)^\lambda$$

is a constant.

By combining (3.6)–(3.8), we have the following:

$$\begin{cases} Q(\hbar(k+1)) \leq \mathcal{N}(\lambda)(1-\hbar\ell_{min}(\Xi))Q(\hbar k) + \hbar\mathcal{N}(\lambda)R(\hbar k) \\ R(\hbar(k+1)) \leq \mathcal{N}(\lambda)(1-\hbar\ell_{min}(A))R(\hbar k) \\ \qquad\qquad + \hbar\mathcal{N}(\lambda)(\|B\| + \|C^*\|\|\|\Psi\|)Q(\hbar k) \\ \qquad\qquad + \hbar\mathcal{N}(\lambda)\left(\dfrac{k+1}{\lfloor \mathfrak{p}k\rfloor + 1}\right)^\lambda (\|D^*\|\|\|\Psi\| + \|\zeta\|)\cdot Q(\lfloor \mathfrak{p}k\rfloor\hbar) \end{cases} \tag{3.9}$$

From (2.2) and $\lfloor \mathfrak{p}k\rfloor > \mathfrak{p}k - 1$, we have $\frac{k+1}{\lfloor \mathfrak{p}k\rfloor+1} < \frac{k+1}{\mathfrak{p}k}$, and it follows that

$$
\begin{cases}
\Delta_\hbar Q(\hbar k) \leq & \dfrac{\mathcal{N}(\lambda)(1-\hbar\ell_{min}(\Xi))-1}{\hbar} Q(\hbar k) + \mathcal{N}(\lambda) R(\hbar k) \\
& \leq \dfrac{\mathcal{N}(\lambda)(1-\hbar\ell_{min}(\Xi))-1}{\hbar} \bar{Q}(\hbar k) + \mathcal{N}(\lambda) \bar{R}(\hbar k), \\
\Delta_\hbar R(\hbar k) \leq & \dfrac{\mathcal{N}(\lambda)(1-\hbar\ell_{min}(A))-1}{\hbar} R(\hbar k) + \mathcal{N}(\lambda)(\|B\| + \|C^*\|\|\Psi\|) Q(\hbar k) \\
& + \mathcal{N}(\lambda)\left(\dfrac{k+1}{\lfloor \mathfrak{p}k \rfloor + 1}\right)^\lambda (\|D^*\|\|\Psi\| + \|\zeta\|) \cdot Q(\lfloor \mathfrak{p}k \rfloor \hbar) \\
& \leq \dfrac{\mathcal{N}(\lambda)(1-\hbar\ell_{min}(A))-1}{\hbar} R(\hbar k) + \mathcal{N}(\lambda)(\|B\| + \|C^*\|\|\Psi\|) Q(\hbar k) \\
& + \mathcal{N}(\lambda)\left(\dfrac{k_0+1}{\tilde{\mathfrak{p}} k_0}\right)^\lambda (\|D^*\|\|\Psi\| + \|\zeta\|) \cdot Q(\lfloor \mathfrak{p}k \rfloor \hbar) \\
& \leq \dfrac{\mathcal{N}(\lambda)(1-\hbar\ell_{min}(A))-1}{\hbar} \bar{R}(\hbar k) + \mathcal{N}(\lambda)\left(\|B\| + \|C^*\|\|\Psi\|\right) \bar{Q}(\hbar k) \\
& + \mathcal{N}(\lambda)\left(\dfrac{k_0+1}{\tilde{\mathfrak{p}} k_0}\right)^\lambda (\|D^*\|\|\Psi\| + \|\zeta\|) \cdot \bar{Q}(\hbar k),
\end{cases}
\tag{3.10}
$$

where

$$
\begin{aligned}
\bar{Q}(\hbar k) &= \max_{s \in [\lfloor \tilde{\mathfrak{p}} k_0 \rfloor, k]_{\mathbb{Z}}} Q(s\hbar) = \max_{s \in [\lfloor \tilde{\mathfrak{p}} k_0 \rfloor, k]_{\mathbb{Z}}} \|e(\hbar s)\| \left(\frac{s+1}{k_0+1}\right)^\lambda, \\
\bar{R}(\hbar k) &= \max_{s \in [\lfloor \tilde{\mathfrak{p}} k_0 \rfloor, k]_{\mathbb{Z}}} R(s\hbar) = \max_{s \in [\lfloor \tilde{\mathfrak{p}} k_0 \rfloor, k]_{\mathbb{Z}}} \|y(\hbar s)\| \left(\frac{s+1}{k_0+1}\right)^\lambda.
\end{aligned}
\tag{3.11}
$$

From (3.7) and (3.11), together with $\Phi = \max\{\bar{\Phi}, (\|I\| + \|\Xi\|)\bar{\Phi}\}$, we have the following:

$$
\begin{cases}
\bar{Q}(\hbar k) \leq \Phi \left(\dfrac{k_0+1}{k_0+1}\right)^\lambda = \Phi, \\
\bar{R}(\hbar k) \leq \Phi \left(\dfrac{k_0+1}{k_0+1}\right)^\lambda = \Phi,
\end{cases}
\quad k \in [\lfloor \tilde{\mathfrak{p}} k_0 \rfloor, k_0]_{\mathbb{Z}}.
\tag{3.12}
$$

Prove that Inequality (3.12) holds in the following conditions:

$$
\begin{cases}
\bar{Q}(\hbar k) \leq \Phi, \\
\bar{R}(\hbar k) \leq \Phi,
\end{cases}
\quad k \in (k_0, +\infty)_{\mathbb{Z}}.
\tag{3.13}
$$

Let $ð > 1$ be an arbitrary constant. First, we prove the following inequality:

$$
\begin{cases}
\bar{Q}(\hbar k) < ð\Phi, \\
\bar{R}(\hbar k) < ð\Phi,
\end{cases}
\quad k \in (k_0, +\infty)_{\mathbb{Z}}.
\tag{3.14}
$$

According to the definition of $\bar{Q}(\hbar k)$, $\bar{Q}(\hbar k) = \max_{s \in [\lfloor \tilde{\mathfrak{p}} k_0 \rfloor, k]_{\mathbb{Z}}} Q(s\hbar)$, we have the following:

$$
\bar{Q}(\hbar(k+1)) = \max\{\bar{Q}(\hbar k), Q(\hbar(k+1))\} \geq \bar{Q}(\hbar k).
$$

Therefore, $\bar{Q}(\hbar k)$ is nondecreasing with respect to the integer index k. Moreover, under the contradiction assumption, there exists at least one integer $k > k_0$ such that $\bar{Q}(\hbar k) \geq ð\Phi$. Therefore, the set of such integer indices is nonempty, and we may define k_* as its smallest element. Then, it follows that

$$\begin{cases} \bar{Q}(\hbar k) < \eth\Phi, \\ \bar{Q}(\hbar k_*) \geq \eth\Phi, \end{cases} \quad k \in [\lfloor \tilde{\mathfrak{p}} k_0 \rfloor, k_* - 1]_{\mathbb{Z}}. \tag{3.15}$$

Hence, we have $\Delta_\hbar \bar{Q}(\hbar k_*) \geq 0$.

Next, we introduce two continuous functions defined by the following:

$$\begin{cases} F(\varpi) = -\mathcal{N}(\varpi) - \dfrac{\mathcal{N}(\varpi)(1 - \hbar\ell_{min}(\Xi)) - 1}{\hbar} = \dfrac{1}{\hbar} - \mathcal{N}(\varpi) - \dfrac{\mathcal{N}(\varpi)(1 - \hbar\ell_{min}(\Xi))}{\hbar}, \\ T(\pi) = -\dfrac{\mathcal{N}(\pi)(1 - \hbar\ell_{min}(A)) - 1}{\hbar} - \mathcal{N}(\pi)\left(\|B\| + \|C^*\|\|\Psi\|\right) - \mathcal{N}(\pi)\left(\dfrac{k_0 + 1}{\tilde{\mathfrak{p}} k_0}\right)^{\pi} \left(\|D^*\|\|\Psi\| + \|\zeta\|\right) \\ \quad = \dfrac{1}{\hbar} - \dfrac{\mathcal{N}(\pi)(1 - \hbar\ell_{min}(A))}{\hbar} - \mathcal{N}(\pi)\left[\|B\| + \|C^*\|\|\Psi\| + \left(\dfrac{k_0 + 1}{\tilde{\mathfrak{p}} k_0}\right)^{\pi} \left(\|D^*\|\|\Psi\| + \|\zeta\|\right)\right], \end{cases} \tag{3.16}$$

where $\varpi \in [0, +\infty)$, $\pi \in [0, +\infty)$, $\mathcal{N}(0) = 1$, and $\mathcal{N}(+\infty) = +\infty$. If the inequalities in (3.1) hold, then we have the following:

$$\begin{cases} \lim\limits_{\varpi \to +\infty} F(\varpi) = -\infty, \quad F(0) > 0, \\ \lim\limits_{\pi \to +\infty} T(\pi) = -\infty, \quad T(0) > 0. \end{cases} \tag{3.17}$$

It follows that there exist two constants $\hat{\varpi}, \hat{\pi} \in (0, +\infty)$ such that

$$\begin{cases} F(\hat{\varpi}) = \dfrac{1}{\hbar} - \mathcal{N}(\hat{\varpi}) - \dfrac{\mathcal{N}(\hat{\varpi})(1 - \hbar\ell_{min}(\Xi))}{\hbar} = 0, \\ T(\hat{\pi}) = \dfrac{1}{\hbar} - \dfrac{\mathcal{N}(\hat{\pi})(1 - \hbar\ell_{min}(A))}{\hbar} - \mathcal{N}(\hat{\pi})\left[\|B\| + \|C^*\|\|\Psi\| + \left(\dfrac{k_0 + 1}{\tilde{\mathfrak{p}} k_0}\right)^{\hat{\pi}} \left(\|D^*\|\|\Psi\| + \|\zeta\|\right)\right] = 0. \end{cases} \tag{3.18}$$

It is easy to choose a constant λ with $0 < \lambda < \min\{\hat{\varpi}, \hat{\pi}\}$ satisfying the following:

$$\begin{cases} F(\lambda) = \dfrac{1}{\hbar} - \mathcal{N}(\lambda) - \dfrac{\mathcal{N}(\lambda)(1 - \hbar\ell_{min}(\Xi))}{\hbar} > 0, \\ T(\lambda) = \dfrac{1}{\hbar} - \dfrac{\mathcal{N}(\lambda)(1 - \hbar\ell_{min}(A))}{\hbar} - \mathcal{N}(\lambda)\left[\|B\| + \|C^*\|\|\Psi\| + \left(\dfrac{k_0 + 1}{\tilde{\mathfrak{p}} k_0}\right)^{\lambda} \left(\|D^*\|\|\Psi\| + \|\zeta\|\right)\right] > 0. \end{cases} \tag{3.19}$$

By (3.10) and (3.19), we have $\Delta_\hbar \bar{Q}(\hbar k_*) < 0$, which contradicts $\Delta_\hbar \bar{Q}(\hbar k_*) \geq 0$ established above. Similarly, the inequality related to $\bar{R}(\hbar k)$ can also be proven by contradiction. Therefore, Inequality (3.13) holds; then, we have the following:

$$\begin{cases} Q(\hbar k) = \|e(\hbar k)\| \left(\dfrac{k + 1}{k_0 + 1}\right)^{\lambda} \leq \bar{Q}(\hbar k) \leq \Phi, \\ R(\hbar k) = \|y(\hbar k)\| \left(\dfrac{k + 1}{k_0 + 1}\right)^{\lambda} \leq \bar{R}(\hbar k) \leq \Phi, \end{cases} \quad k \in [\lfloor \mathfrak{p} k_0 \rfloor, +\infty)_{\mathbb{Z}}. \tag{3.20}$$

Then,

$$\begin{cases} \|e(\hbar k)\| \leq \Phi \left(\dfrac{k + 1}{k_0 + 1}\right)^{-\lambda}, \\ \|y(\hbar k)\| \leq \Phi \left(\dfrac{k + 1}{k_0 + 1}\right)^{-\lambda}, \end{cases} \quad k \in [\lfloor \mathfrak{p} k_0 \rfloor, +\infty)_{\mathbb{Z}}. \tag{3.21}$$

From Definition 1 and (3.1), it follows that the drive-response Systems (2.3) and (2.4) achieve GPS. This completes the proof. □

Remark 4. *The unboundedness of proportional delays has long been a major challenge in the analysis of such systems. Most existing results on proportional-delay NNs are obtained for continuous-time systems, where logarithmic transformations are often used to transform proportional delays into constant delays [27–29]. Recently, Li and Chen [30] investigated the discrete-time analogues of continuous-time quaternion-valued NNs with proportional delays using the semi-discretization method. In their approach, the continuous delay length* $(1-q_j)t$ *is discretized as* $T_j = [(1-q_j)t/h]$*, thus leading to the delayed term* $Z_j(k-T_j)$*. In contrast, Model (2.1) is directly established on the sampling time scale kh, and the proportional delay is represented by* $x_j(\lfloor \mathfrak{p}k \rfloor \hbar)$*. To the best of our knowledge, few results have directly treated proportional delays in the discrete-time neural network framework.*

From (3.19), we establish the following delay-dependent criterion for GPS.

Theorem 2. *Suppose Assumptions 1 and 2 hold; for a given* $k_0 > 0$, $\mathcal{N}(\lambda) = \left(\frac{k_0+2}{k_0+1}\right)^{\lambda}$, $\Phi = \max\{\bar{\Phi}, (\|I\| + \|\Xi\|)\bar{\Phi}\}$*, and* $\Psi = \mathrm{diag}\{\psi_1, \psi_2, \ldots, \psi_n\}$*, the drive-response PD-DTINNs (2.3) and (2.4) achieve GPS under Controller (2.6) if there is a constant* $\lambda > 0$ *such that*

$$\begin{cases} \mathcal{N}(\lambda) + \dfrac{\mathcal{N}(\lambda)(1-\hbar\ell_{min}(\Xi))}{\hbar} < \dfrac{1}{\hbar}, \\ \dfrac{\mathcal{N}(\lambda)(1-\hbar\ell_{min}(A))}{\hbar} + \mathcal{N}(\lambda)\left[\|B\| + \|C^*\|\|\Psi\| + \left(\dfrac{k_0+1}{\tilde{\mathfrak{p}}k_0}\right)^{\lambda}(\|D^*\|\|\Psi\| + \|\zeta\|)\right] < \dfrac{1}{\hbar}. \end{cases} \tag{3.22}$$

For any $\lambda = 0$, the following GAS result is an immediate consequence of Theorem 2.

Corollary 1. *Suppose Assumptions 1 and 2 hold; for a given* $\Psi = \mathrm{diag}\{\psi_1, \psi_2, \ldots, \psi_n\}$*, the drive-response PD-DTINNs (2.3) and (2.4) achieve GAS under Controller (2.6) if the following conditions hold:*

$$\begin{cases} \ell_{min}(\Xi) > 1, \\ \ell_{min}(A) > \|B\| + \|C^*\|\|\Psi\| + \|D^*\|\|\Psi\| + \|\zeta\|. \end{cases} \tag{3.23}$$

Remark 5. *Theorem 1 presents a delay-independent criterion for GPS. Although neither the proportional-delay factors nor the decay rate explicitly appears in its conditions, and the strict inequalities guarantee the existence of an admissible* $\lambda > 0$*. Theorem 2, by contrast, explicitly involves both* λ *and the proportional-delay factors and therefore gives a more direct description of the admissible polynomial decay rate. Corollary 1 establishes a GAS criterion under different sufficient conditions. As mentioned in the Introduction, the existing results on GPS have mainly been developed for continuous-time systems [17,19,20]. The present results extend this type of synchronization analysis to discrete-time INNs with proportional delays. Moreover, polynomial decay is naturally compatible with the increasing-lag feature of proportional delays, which facilitates their direct treatment in the discrete-time framework.*

To further investigate the stability of the considered system, we next consider the corresponding single System (2.3). By following the proof strategy of Theorem 1 with some necessary modifications, the global polynomial stability and global asymptotic stability criteria can be established. The details are given as follows.

By applying the reduced-order method to PD-DTINNs (2.3) and using the variable transformation $r(\hbar k) = \Delta_\hbar x(\hbar k) + \Xi x(\hbar k)$, we obtain the following:

$$\begin{cases} \Delta_\hbar x(\hbar k) = -\Xi x(\hbar k) + r(\hbar k), \\ \Delta_\hbar r(\hbar k) = -\mathcal{A} r(\hbar k) - \mathcal{B} x(\hbar k) + C^* f(x(\hbar k)) + D^* f(x(\lfloor \mathfrak{p} k \rfloor \hbar)) + R^*, \end{cases} \tag{3.24}$$

where $\mathcal{A} = A^* - \Xi$, $\mathcal{B} = -\Xi A^* + \Xi^2 + B^*$. Let $(\bar{x}, \bar{r})$ be the equilibrium point of PD-DTINNs (3.24), with $\bar{x} = (\bar{x}_1, \bar{x}_2, ..., \bar{x}_n)^T, \bar{r} = (\bar{r}_1, \bar{r}_2, ..., \bar{r}_n)^T$. Then, we have the following:

$$\begin{cases} \Delta_\hbar \hat{x}(\hbar k) = -\Xi \hat{x}(\hbar k) + \hat{r}(\hbar k), \\ \Delta_\hbar \hat{r}(\hbar k) = -\mathcal{A} \hat{r}(\hbar k) - \mathcal{B} \hat{x}(\hbar k) + C^* f(\hat{x}(\hbar k)) + D^* f(\hat{x}(\lfloor \mathfrak{p} k \rfloor \hbar)), \end{cases} \tag{3.25}$$

where

$$\hat{x}(\hbar k) = x(\hbar k) - \bar{x}, \hat{r}(\hbar k) = r(\hbar k) - \bar{r},$$

$$f(x(\hbar k)) = g(x(\hbar k)) - g(\bar{x}),$$

$$f(x(\lfloor \mathfrak{p} k \rfloor \hbar)) = g(x(\lfloor \mathfrak{p} k \rfloor \hbar)) - g(\bar{x}).$$

Define the following:

$$\begin{cases} \check{\varphi} = \max\limits_{s \in [\lfloor \tilde{\mathfrak{p}} k_0 \rfloor, k_0]_{\mathbb{Z}}} \|\varphi(s\hbar)\| \\ \check{\phi} = \max\limits_{s \in [\lfloor \tilde{\mathfrak{p}} k_0 \rfloor, k_0]_{\mathbb{Z}}} \|\phi(s\hbar)\| \end{cases} \tag{3.26}$$

where $\varphi(s\hbar)$, and $\phi(s\hbar)$ is the initial value of PD-DTINNs (2.3), either $\check{\varphi}$ or $\check{\phi}$ is positive. For example, if $\check{\varphi} > 0$, then we can make $\check{\phi} = 0$. Denote $\bar{\Theta} = \max\{\check{\varphi}, \check{\phi}\}$. According to $r(\hbar k) = \Delta_\hbar x(\hbar k) + \Xi x(\hbar k)$, it is easy to obtain $\max_{s \in [\lfloor \tilde{\mathfrak{p}} k_0 \rfloor, k_0]_{\mathbb{Z}}} \|r(s\hbar)\| \leq (\|I\| + \|\Xi\|)\bar{\Theta} \leq \Theta$, with $\Theta = \max\{\bar{\Theta}, (\|I\| + \|\Xi\|)\bar{\Theta}\}$.

According to the above analysis and the proof strategy of Theorem 1, the following Corollaries 2 and 3 were established.

Corollary 2. *Suppose Assumption 1 holds; for a given* $k_0 > 0$, $\mathcal{N}(\lambda) = \left(\frac{k_0+2}{k_0+1}\right)^\lambda$, $\Theta = \max\{\bar{\Theta}, (\|I\| + \|\Xi\|)\bar{\Theta}\}$, *and* $\Psi = \mathrm{diag}\{\psi_1, \psi_2, \ldots, \psi_n\}$, *PD-DTINNs (2.3) are globally polynomial stable if there is a constant* $\lambda > 0$ *such that*

$$\begin{cases} \mathcal{N}(\lambda) + \dfrac{\mathcal{N}(\lambda)(1 - \hbar \ell_{min}(\Xi))}{\hbar} < \dfrac{1}{\hbar}, \\ \dfrac{\mathcal{N}(\lambda)(1 - \hbar \ell_{min}(\mathcal{A}))}{\hbar} + \mathcal{N}(\lambda) \left[\|\mathcal{B}\| + \|C^*\| \|\Psi\| + \left(\dfrac{k_0 + 1}{\tilde{\mathfrak{p}} k_0} \right)^\lambda \|D^*\| \|\Psi\| \right] < \dfrac{1}{\hbar}. \end{cases} \tag{3.27}$$

Corollary 3. *Suppose Assumption 1 holds; for a given* $\Psi = \mathrm{diag}\{\psi_1, \psi_2, \ldots, \psi_n\}$, *PD-DTINNs(2.3) are globally asymptotic stable if the following conditions hold:*

$$\begin{cases} \ell_{min}(\Xi) > 1, \\ \ell_{min}(\mathcal{A}) > \|\mathcal{B}\| + \|C^*\| \|\Psi\| + \|D^*\| \|\Psi\|. \end{cases} \tag{3.28}$$

4. Numerical examples

Example 1. *The following PD-DTINNs are considered, with System (4.1) as the drive system and System (4.2) as the response system:*

$$\begin{cases} \Delta_\hbar^2 x_1(\hbar k) = -0.44\Delta_\hbar x_1(\hbar k) - 1.6x_1(\hbar k) + 0.2g_1(x_1(\hbar k)) + 0.1g_2(x_2(\hbar k)) \\ \qquad\qquad - 0.1g_1(x_1(\lfloor 0.5k \rfloor \hbar)) + 0.1g_2(x_2(\lfloor 0.6k \rfloor \hbar)) + 0.4\sin(\hbar k), \\ \Delta_\hbar^2 x_2(\hbar k) = -0.45\Delta_\hbar x_2(\hbar k) - 1.8x_2(\hbar k) - 0.1g_1(x_1(\hbar k)) + 0.2g_2(x_2(\hbar k)) \\ \qquad\qquad - 0.1g_1(x_1(\lfloor 0.5k \rfloor \hbar)) + 0.1g_2(x_2(\lfloor 0.6k \rfloor \hbar)) + 0.4\cos(\hbar k), \end{cases} \tag{4.1}$$

$$\begin{cases} \Delta_\hbar^2 \eta_1(\hbar k) = -0.44\Delta_\hbar \eta_1(\hbar k) - 1.6\eta_1(\hbar k) + 0.2g_1(\eta_1(\hbar k)) + 0.1g_2(\eta_2(\hbar k)) \\ \qquad\qquad - 0.1g_1(\eta_1(\lfloor 0.5k \rfloor \hbar)) + 0.1g_2(\eta_2(\lfloor 0.6k \rfloor \hbar)) + 0.4\sin(\hbar k) + \mathcal{K}_1(\hbar k), \\ \Delta_\hbar^2 \eta_2(\hbar k) = -0.45\Delta_\hbar \eta_2(\hbar k) - 1.8\eta_2(\hbar k) - 0.1g_1(\eta_1(\hbar k)) + 0.2g_2(\eta_2(\hbar k)) \\ \qquad\qquad - 0.1g_1(\eta_1(\lfloor 0.5k \rfloor \hbar)) + 0.1g_2(\eta_2(\lfloor 0.6k \rfloor \hbar)) + 0.4\cos(\hbar k) + \mathcal{K}_2(\hbar k). \end{cases} \tag{4.2}$$

Then, we can have the error system as follows:

$$\begin{cases} \Delta_\hbar^2 e_1(\hbar k) = -0.44\Delta_\hbar e_1(\hbar k) - 1.6e_1(\hbar k) + 0.2g_1(e_1(\hbar k)) + 0.1g_2(e_2(\hbar k)) \\ \qquad\qquad - 0.1g_1(e_1(\lfloor 0.5k \rfloor \hbar)) + 0.1g_2(e_2(\lfloor 0.6k \rfloor \hbar)) + \mathcal{K}_1(\hbar k), \\ \Delta_\hbar^2 e_2(\hbar k) = -0.45\Delta_\hbar e_2(\hbar k) - 1.8e_2(\hbar k) - 0.1g_1(e_1(\hbar k)) + 0.2g_2(e_2(\hbar k)) \\ \qquad\qquad - 0.1g_1(e_1(\lfloor 0.5k \rfloor \hbar)) + 0.1g_2(e_2(\lfloor 0.6k \rfloor \hbar)) + \mathcal{K}_2(\hbar k). \end{cases} \tag{4.3}$$

Let Ξ =diag$\{1.34, 1.44\}$, set $\hbar = 0.25$, $k_0 = 1$, $g_1(k) = g_2(k) = 0.1\tanh(\hbar k)$, and the initial values $\varphi(s\hbar) = \{-1.1, 1.3\}$ of the drive system and $\bar{\varphi}(s\hbar) = \{3.4, 4.4\}$ of the response system. Figure 1 shows the phase diagram of the uncontrolled drive System (4.1), from which complex and irregular dynamical behaviors can be observed. Furthermore, Figure 2 presents the state responses of the drive-response PD-DTINNs (4.1) and (4.2) without control, while Figure 3 shows the corresponding error responses. The state responses of the two systems do not coincide, and the synchronization errors fail to converge to zero.

Then, we choose the control gains in Controller (2.6) as follows:

$$\alpha = \begin{bmatrix} -3.19 & 0 \\ 0 & -3.63 \end{bmatrix}, \quad \beta = \begin{bmatrix} 2.01 & 0 \\ 0 & 1.98 \end{bmatrix}, \quad \zeta = \begin{bmatrix} 0.02 & 0.01 \\ 0.02 & 0.01 \end{bmatrix}.$$

Under the controller and $A = A^* - \Xi + \beta$, $B = -\Xi A^* + \Xi^2 + B^* + \alpha$, System (4.3) can be expressed in the form of (2.7) with the corresponding matrices given as follows:

$$A = \begin{bmatrix} 1.11 & 0 \\ 0 & 0.99 \end{bmatrix}, \quad B = \begin{bmatrix} 0.374 & 0 \\ 0 & 0.4044 \end{bmatrix}, \quad C^* = \begin{bmatrix} 0.2 & 0.1 \\ -0.1 & 0.2 \end{bmatrix}, D^* = \begin{bmatrix} -0.1 & 0.1 \\ -0.1 & 0.1 \end{bmatrix}.$$

After calculation, we have $\Phi = \max\{\bar{\Phi}, (\|I\| + \|\Xi\|)\bar{\Phi}\} \geq \max\{4.5, 3.1\}$, $\ell_{min}(\Xi) = 1.34$, $1 + \frac{1}{\hbar} = 5$, $\ell_{min}(A) = 0.9900$, and $\|B\| + \|C^*\| \cdot \|\Psi\| + \|D^*\| \cdot \|\Psi\| + \|\zeta\| = 0.4784$. Clearly, Condition (3.1) of Theorem 1 is satisfied, and the drive–response PD-DTINNs can achieve GPS. Furthermore, as shown in Figures 4 and 5, the response System (4.2) successfully tracks the drive System (4.1) under the designed controller.

Subsequently, by $\tilde{\mathfrak{p}} = \min\{0.5, 0.6\} = 0.5$ and let $\lambda = 0.14$, we can obtain that

$$\begin{cases} \mathcal{N}(\lambda) + \dfrac{\mathcal{N}(\lambda)(1 - \hbar\ell_{min}(\Xi))}{\hbar} = 3.8738 < \dfrac{1}{\hbar} = 4, \\ \dfrac{\mathcal{N}(\lambda)(1 - \hbar\ell_{min}(A))}{\hbar} + \mathcal{N}(\lambda)\left[||B|| + ||C^*||||\Psi|| + \left(\dfrac{k_0 + 1}{\tilde{\mathfrak{p}}k_0}\right)^{\lambda}(||D^*||||\Psi|| + ||\zeta||)\right] = 3.7038 < \dfrac{1}{\hbar} = 4. \end{cases}$$

According to Theorem 2, Condition (3.22) is satisfied, which indicates the drive–response PD-DTINNs (4.1) and (4.2) can achieve GPS with a guaranteed decay rate of $\lambda = 0.14$.

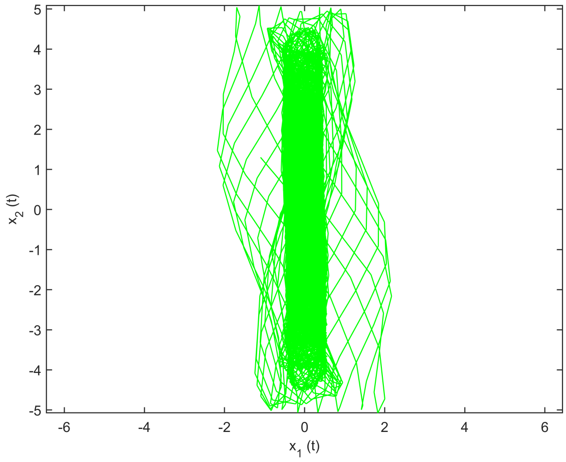

Figure 1. Phase plot of drive system (4.1).

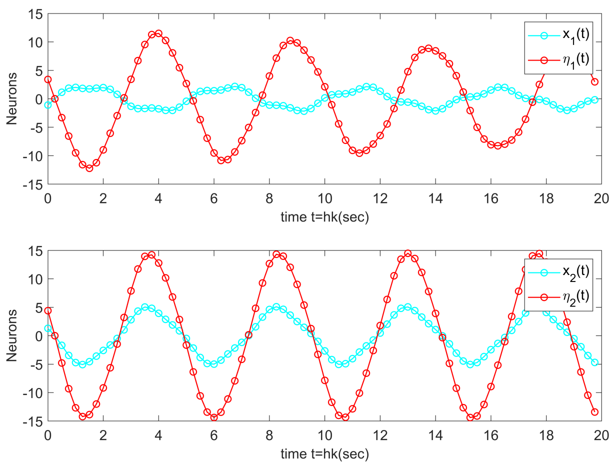

Figure 2. Unsynchronized state responses of drive System (4.1) and response System (4.2) without control.

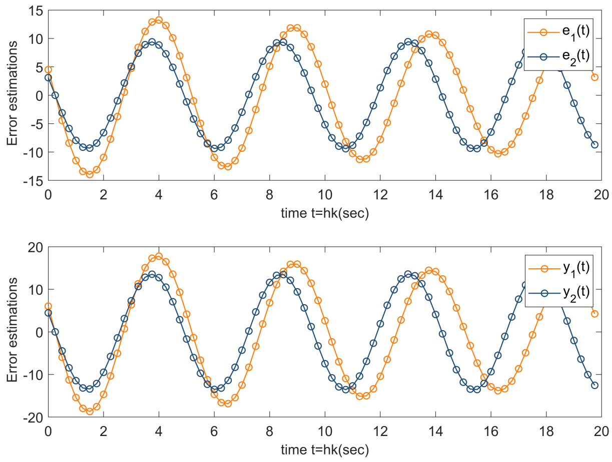

Figure 3. State responses of the error System (4.3) without control, $i = 1, 2$.

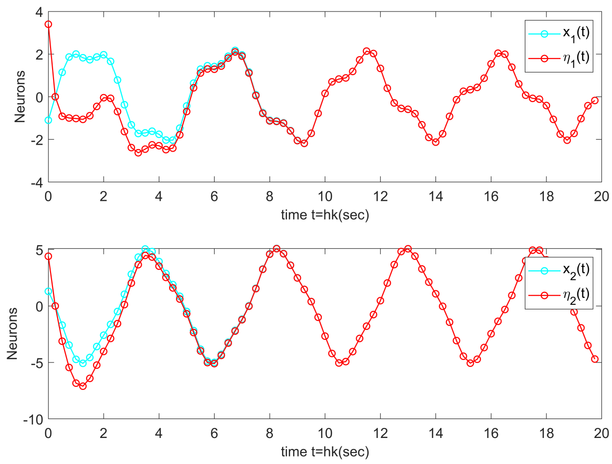

Figure 4. Synchronized state responses of $x_i(\hbar k)$ and $\eta_i(\hbar k)$ under Controller (2.6), $i = 1, 2$.

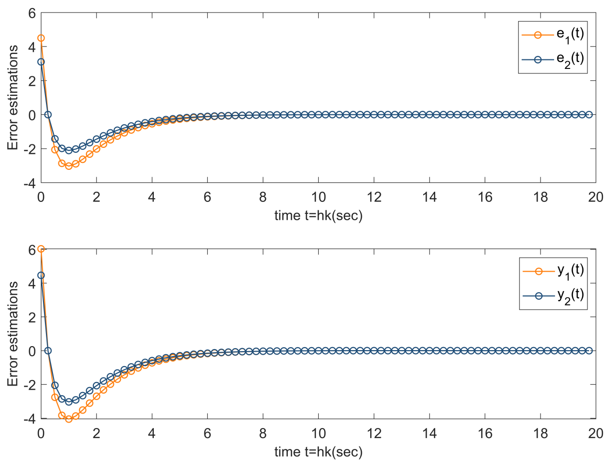

Figure 5. State responses of the error System (4.3) under Controller (2.6), $i = 1, 2$.

Example 2. *In this example, the synchronization criterion obtained in Theorem 1 is applied to image encryption. The state sequences generated by Systems (4.1) and (4.2) are used to encrypt and decrypt image Q ('Cat.png'), and the corresponding process is described as follows.*

P1 (Initial image preprocessing): Input a color image $Q \in \mathbb{R}^{256\times256\times3}$. The pixel values of the original image are read and decomposed into three color channels, namely red, green, and blue. These three channels are represented by matrices $R = (r_{ij})_{n\times m}, G = (g_{ij})_{n\times m}$, and $B = (b_{ij})_{n\times m}$, respectively, where $n, m \in [1, 256]$.

P2 (Chaotic sequence generation): After discarding the transient iterations before k_s where the synchronization error is sufficiently small $(\|e(\hbar k_s)\| \le 10^{-4})$, the state sequences $x_1(\hbar k)$ and $x_2(\hbar k)$ for $k \ge k_s$ are extracted to generate the following chaotic sequence:

$$
\begin{aligned}
u_1(i) &= \{x_1(\hbar k_i)\}_{k_i}^{k_{i+nm}}, \quad k_s \le k_i, \\
u_2(j) &= \{x_2(\hbar k_j)\}_{k_j}^{k_{j+nm}}, \quad k_s \le k_j.
\end{aligned} \tag{4.4}
$$

P3 (Generation of three encryption matrices): The chaotic sequence is preprocessed to generate three encryption matrices K_R, K_G, K_B according to the following operations:

$$
\begin{aligned}
K_R &= \mathrm{mod}\left(\mathrm{round}\left(|u_1 - 2u_2| \times 10^8\right), 256\right), \\
K_G &= \mathrm{mod}\left(\mathrm{round}\left(|2u_1 - u_2| \times 10^8\right), 256\right), \\
K_B &= \mathrm{mod}\left(\mathrm{round}\left(|u_1 + 2u_2| \times 10^8\right), 256\right).
\end{aligned}
$$

These different operations help generate independent keys for the three color channels.

P4 (Encryption): The encryption procedure is split into pixel scrambling, cross-channel diffusion, and final XOR masking three stages. The pixel matrices of three channels are reshaped into one-dimensional sequences:

$$
\boldsymbol{r} = \mathrm{reshape}(R, 1, \mathcal{L}), \quad \boldsymbol{g} = \mathrm{reshape}(G, 1, \mathcal{L}), \quad \boldsymbol{b} = \mathrm{reshape}(B, 1, \mathcal{L}), \qquad \mathcal{L} = nm,
$$

where $\mathcal{L}$ denotes the total pixel quantity of a single channel.

S1. Scrambling: Sort the chaotic sequence u_1 to get the sorting index array $\boldsymbol{idx}_{\mathrm{sort}}$:

$$
\boldsymbol{idx}_{\mathrm{sort}} = \mathrm{sort}(u_1).
$$

Perform index permutation for three channels: $r_p = \boldsymbol{r}(\boldsymbol{idx}_{\mathrm{sort}})$, $g_p = \boldsymbol{g}(\boldsymbol{idx}_{\mathrm{sort}})$, $b_p = \boldsymbol{b}(\boldsymbol{idx}_{\mathrm{sort}})$.

S2. Cross-channel coupled diffusion: Set initial boundary $r_{d,1} = r_{p,1}$, $g_{d,1} = g_{p,1}$, $b_{d,1} = b_{p,1}$. For $t = 2, 3, \ldots, \mathcal{L}$, iterative diffusion is performed as follows:

$$
\begin{aligned}
r_{d,t} &= \mathrm{mod}\ (r_{p,t} + 2r_{d,t-1} + 2g_{d,t-1} + 2b_{d,t-1} + 7|u_2(t)|,\ 1), \\
g_{d,t} &= \mathrm{mod}\ (g_{p,t} + 2g_{d,t-1} + 2r_{d,t-1} + 2b_{d,t-1} + 7|u_1(t)|,\ 1), \\
b_{d,t} &= \mathrm{mod}\ (b_{p,t} + 2b_{d,t-1} + 2r_{d,t-1} + 2g_{d,t-1} + 7|u_1(t) + u_2(t)|,\ 1).
\end{aligned}
$$

Map normalized diffused values back into the integer interval $[0, 255]$.

S3. XOR masking: The final encrypted pixel matrices $\tilde{R} = (\tilde{r}_{ij})_{n\times m}$, $\tilde{G} = (\tilde{g}_{ij})_{n\times m}$, $\tilde{B} = (\tilde{b}_{ij})_{n\times m}$ are obtained by the following XOR operations:

$$\tilde{r}_{ij} = R_d(i,j)\,\text{bitxor}\,K_R(i,j),\quad \tilde{g}_{ij} = G_d(i,j)\,\text{bitxor}\,K_G(i,j),\quad \tilde{b}_{ij} = B_d(i,j)\,\text{bitxor}\,K_B(i,j).$$

Then, $\tilde{R}, \tilde{G}$ and $\tilde{B}$ are combined to reconstruct the encrypted color image $\tilde{Q}$.

P5 (Decryption): Regenerate the identical chaotic sequences u_1, u_2 and key matrices K_R, K_G, K_B from the synchronized response System (4.2). The decryption strictly follows the reverse order of P4:inverse XOR operation, backward iterative diffusion, and inverse index scrambling. The relevant derivation is omitted here for brevity.

Key space is the full collection of all valid keys supported by a encryption algorithm. The encryption matrices K_R, K_G, K_B are generated by the PD-DTINNs in Example 1, where the system parameters A^*, B^*, C^*, D^*, delay factor $\mathfrak{p}_j$, sampling step size $\hbar$, initial conditions φ, ϕ, synchronization instant k_s, and control gain α,β,ζ belong to completely independent and adjustable parameters, which can be treated as the secret keys. In contrast to the first-order system in [19], the second-order PD-DTINNs framework investigated in this work exhibits richer dynamical complexity. That means that the proposed encryption scheme has a larger key space and is easier to defend the brute-force attacks.

Figure 6 gives the visual results of the original, encrypted, and decrypted images, while Figure 7 presents the RGB-channel histograms. It can be seen from Figure 6(b) that the encrypted image becomes noise-like, and the main visual contents of the original image are no longer recognizable. In addition, the histograms of the encrypted image in Figure 7(b),(e),(h) are much flatter than those of the original image, thus indicating that the pixel values are more evenly distributed after encryption. Therefore, the proposed encryption scheme can effectively mask the statistical characteristics of the original image and improve the resistance to statistical analyses.

Figures 8 and 9 present the adjacent-pixel correlation plots of the original and encrypted images, respectively, in the horizontal, vertical, and diagonal directions. In Figure 8, the data points are concentrated around a linear pattern, thus indicating strong adjacent-pixel correlation in the original image. After encryption, as shown in Figure 9, the data points become randomly scattered and the correlation coefficients are close to zero. This shows that the proposed encryption scheme can effectively reduce the adjacent-pixel correlation.

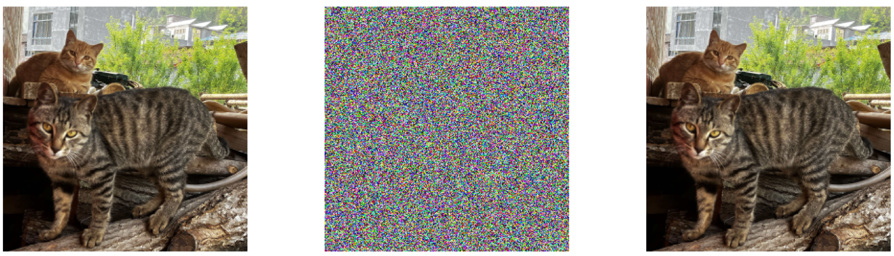

(a) (b) (c)

Figure 6. (a) Initial image; (b) Encryption image; (c) Decryption image.

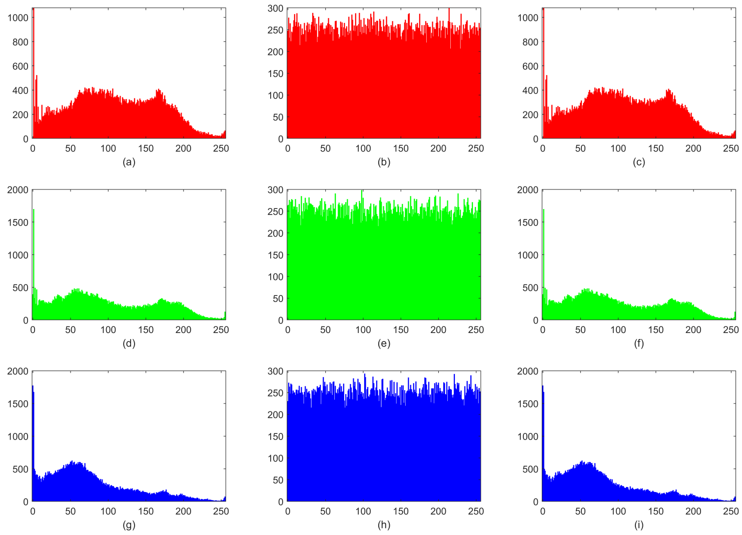

Figure 7. Histograms of the RGB channels: (a,d,g) original image; (b,e,h) encrypted image; (c,f,i) decrypted image.

As shown in Figures 8 and 9, Table 1 gives the Pearson correlation coefficients of adjacent pixels in the horizontal, vertical, and diagonal directions for the RGB channels of the original and encrypted images. The coefficients of the original image are close to 1, whereas those of the encrypted image are close to 0. Moreover, the scatter plots change from a concentrated near-linear pattern to a more uniformly scattered distribution. This confirms that the proposed encryption algorithm effectively weakens adjacent-pixel correlations and improves resistance to statistical analysis attacks.

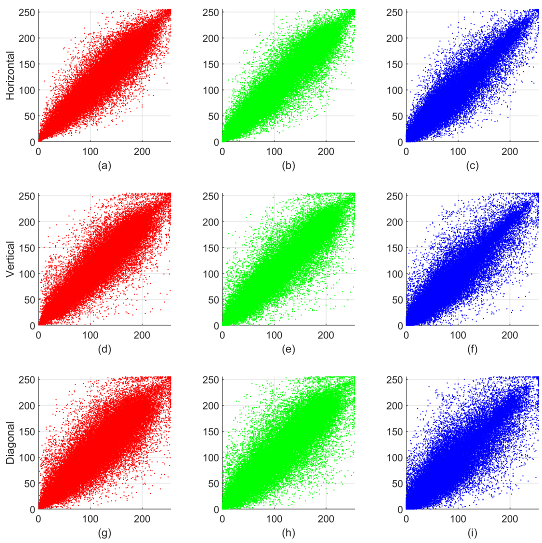

Figure 8. Scatter plots of adjacent pixels in the horizontal, vertical, and diagonal directions for the R, G, and B channels of the plain image.

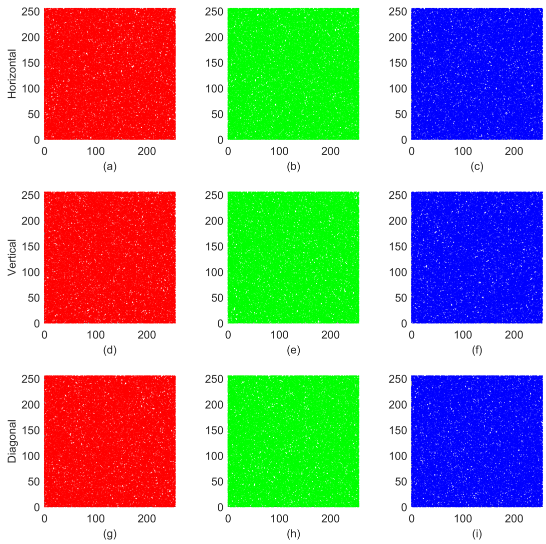

Figure 9. Scatter plots of adjacent pixels in the horizontal, vertical, and diagonal directions for the R, G, and B channels of the encrypted image.

Table 1. Correlation coefficients of adjacent pixels.

Image	Channel	Horizontal	Vertical	Diagonal
The original image	R	0.9463	0.9315	0.8992
	G	0.9534	0.9401	0.9123
	B	0.9451	0.9267	0.8937
The encryption image	R	-0.0044	0.0045	-0.0036
	G	0.0042	-0.0024	-0.0011
	B	0.0056	0.0019	-0.0008

Information entropy is used here to measure the randomness of pixel values after encryption. For an 8-bit image, it is defined as follows:

$$\mathcal{G}(l) = \sum_{i=0}^{255} p(l_i) \log_2 p(l_i),$$

where $p(l_i)$ denotes the probability of gray level l_i. The theoretical maximum is 8; hence, a value close to 8 suggests that the encrypted image has a nearly random gray-level distribution.

Table 2 shows that the entropy value of the encrypted image is very close to 8. This result suggests that the pixel distribution after encryption is nearly random. Combined with the previous visual and histogram results, the proposed scheme can effectively hide the original image information and provides a feasible encryption strategy.

As two important indicators for resisting differential attacks in cryptographic algorithms, the Number of Pixels Change Rate (NPCR) and the Unified Average Changing Intensity (UACI) can be mathematically obtained as

$$NPCR = \frac{\sum_{i=1}^{m} \sum_{j=1}^{n} Q(i, j)}{n \times m} \times 100\%,$$
$$UACI = \frac{\sum_{i=1}^{m} \sum_{j=1}^{n} |(Q_1(i, j) - Q_2(ia, j)|}{n \times m \times 255} \times 100\%,$$

where, m and n represent the dimensions of the image, while $Q_1(i, j)$ and $Q_2(i, j)$ denote the pixel values at the location (i, j) in the encrypted images Q_1 and Q_2, respectively. One is derived from the original image, and the other is derived from a modified version with a single pixel change. When $Q_1(i, j) \neq Q_2(i, j), Q(i, j) = 1$; otherwise, $Q(i, j) = 0$. For 256×256 images, effective encryption is characterized by an expected NPCR value not below 99.5693 and the UACI target value is range between 33.2823 and 33.6447.

Table 2. Information entropy of the original and encrypted images.

image	R-channel	G-channel	B-channel
The original image	7.7678	7.7674	7.5035
The encryption image	7.9974	7.9973	7.9976

The NPCR and UACI values of this paper are presented in Table 3, which demonstrates that changing a pixel value in each channel yields NPCR and UACI values near the optimal level. This verifies that our encryption algorithm has excellent plaintext sensitivity, and highlights the strong robustness and reliable differential resistance of the proposed method.

Table 3. NPCR and UACI values.

Image	NPCR(%)			UACI(%)		
	R	G	B	R	G	B
Cat	99.6340	99.6032	99.6278	33.4358	33.4652	33.3836

5. Conclusions

In this paper, the GPS problem was studied for PD-DTINNs. The proportional-delay term was directly handled on the discrete sampling grid, which provides a natural framework to describe proportional delays in discrete-time systems. A simple feedback controller was introduced, and a direct analytical method based on auxiliary functions, difference relations, and norm estimates was developed. Within the proposed framework, both delay-dependent and delay-independent criteria for GPS were established, and the corresponding GAS conclusions were obtained. Additionally, the analytical results were extended to the global polynomial and asymptotic stability of a single discrete-time proportional-delay inertial neural network.

The numerical simulation confirmed the validity of the derived criteria. Moreover, the synchronization results were used to construct an image encryption and decryption scheme. The visual results and security analyses, including the key space, histograms, adjacent-pixel correlations, information entropy, and differential attack analysis, demonstrated that the proposed scheme can effectively hide the image information and has potential value in image security. Future research may extend the present framework to more general PD-DTINNs involving parameter uncertainties, switching structures or stochastic disturbances, as well as their synchronization under event-triggered or sampled-data control.

Author contributions

Fengzhao Wang: Formal analysis (equal); Software (equal); Writing – original draft (equal); Xingjian Chen: Writing – original draft (equal); Validation (equal); Cheng Yang: Writing review and editing (equal); Xuan Chen: Funding acquisition (equal); Investigation (equal); Methodology (equal). All authors have read and approved the final version of the manuscript for publication.

Use of Generative-AI tools declaration

The authors declare they have not used Artificial Intelligence (AI) tools in the creation of this article.

Acknowledgments

This study was supported by the Guizhou Provincial Science and Technology Foundation [Grant No. ZK(2023)255, ZD(2026)109], and National Nature Science Foundation of China (No. 62562018).

Conflict of interest

The authors have no conflicts of interest to disclose.

References

1. F. Zhang, P. Gao, T. Huang, Z. Zeng, Stability and associative memories of multi-layer memristive neural networks in the flux-charge domain, *Neurocomputing,* **650** (2025), 130817. https://doi.org/10.1016/j.neucom.2025.130817
2. F. Wei, G. Chen, Z. Zeng, N. Gunasekaran, Finite/fixed-time synchronization of inertial memristive neural networks by interval matrix method for secure communication, *Neural Networks*, **167** (2023), 168–182. https://doi.org/10.1016/j.neunet.2023.08.015
3. Y. Yang, D. Li, H. Li, D. Li, Joint probability distribution of weather factors: a neural network approach for environmental science, *Stoch. Environ. Res. Risk Assess.*, **37** (2023), 4385–4397. https://doi.org/10.1007/s00477-023-02513-1
4. K. L. Babcock, R. M. Westervelt, Stability and dynamics of simple electronic neural networks with added inertia, *Phys. D*, **28** (1986), 464–469. https://doi.org/10.1016/0167-2789(86)90152-1
5. P. Liu, J. Yong, J. Zhao, J. Sun, Synchronization of coupled inertial neural networks via continuous and event-triggered pinning controls, *J. Franklin Inst.*, **361** (2024), 106869. https://doi.org/10.1016/j.jfranklin.2024.106869
6. W. Yao, C. Wang, Y. Sun, S. Gong, H. Lin, Event-triggered control for robust exponential synchronization of inertial memristive neural networks under parameter disturbance, *Neural Networks*, **164** (2023), 67–80. https://doi.org/10.1016/j.neunet.2023.04.024

7. L. Duan, J. Li, Finite-time synchronization for a fully complex-valued BAM inertial neural network with proportional delays via non-reduced order and non-separation approach, *Neurocomputing*, **611** (2024), 128648. https://doi.org/10.1016/j.neucom.2024.128648
8. J. Tong, M. Jiang, Fixed-time synchronization of memristive neural networks with time-varying delays via a new stability criterion, *AIMS Math.*, **11** (2026), 7633–7658. https://doi.org/10.3934/math.2026314
9. Z. Dong, J. Shen, C. Lian, S. Wang, Event-triggered global synchronization control of discrete-time delayed neural networks with applications in image encryption, *J. Franklin Inst.*, **363** (2026), 108524. https://doi.org/10.1016/j.jfranklin.2026.108524
10. X. Chen, D. Lin, Stabilization for a class of delayed switched inertial neural networks via non-reduced order method, *Trans. Inst. Meas. Control*, **43** (2021), 1949–1957. https://doi.org/10.1177/0142331220985944
11. X. Chen, D. Lin, W. Lan, Global dissipativity of delayed discrete-time inertial neural networks, *Neurocomputing*, **390** (2020), 131–138. https://doi.org/10.1016/j.neucom.2020.01.073
12. Y. Shen, X. Liu, W. Li, Finite-time synchronization of complex-valued neural networks via hybrid impulsive control with distributed delays, *Neurocomputing*, **685** (2026), 133576. https://doi.org/10.1016/j.neucom.2026.133576
13. J. Liu, H. L. Li, C. Hu, H. Jiang, J. Cao, Complete synchronization of discrete-time fractional-order BAM neural networks with leakage and discrete delays, *Neural Networks*, **180** (2024), 106705. https://doi.org/10.1016/j.neunet.2024.106705
14. T. Zhang, L. Wang, Y. Zhang, J. Deng, Finite-time stability for fractional-order fuzzy neural network with mixed delays and inertial terms, *AIMS Math.*, **9** (2024), 19176–19194. https://doi.org/10.3934/math.2024935
15. L. Zhou, Global asymptotic stability of cellular neural networks with proportional delays, *Nonlinear Dyn.*, **77** (2014), 41–47. https://doi.org/10.1007/s11071-014-1271-y
16. L. Zhou, Global exponential dissipativity of impulsive recurrent neural networks with multi-proportional delays, *Neural Process. Lett.*, **53** (2021), 1435–1452. https://doi.org/10.1007/s11063-021-10451-8
17. X. Mao, Almost sure polynomial stability for a class of stochastic differential equations, *Q. J. Math.*, **43** (1992), 339–348. https://doi.org/10.1093/qmath/43.3.339
18. L. Zhou, Z. Zhao, Exponential synchronization and polynomial synchronization of recurrent neural networks with and without proportional delays, *Neurocomputing*, **372** (2020), 109–116. https://doi.org/10.1016/j.neucom.2019.09.046
19. Y. Wan, L. Zhou, J. Han, Global polynomial synchronization of proportional delay memristive neural networks with uncertain parameters and its application to image encryption, *Eng. Appl. Artif. Intel.*, **147** (2025), 110290. https://doi.org/10.1016/j.engappai.2025.110290
20. Y. Guo, L. Zhou, Global polynomial synchronization of uncertain complex-valued reaction–diffusion T–S fuzzy memristive neural networks with proportional delays under adaptive event-triggered control, *IEEE Trans. Neural Net. Lear. Syst.*, 2026, 1–12. https://doi.org/10.1109/tnnls.2026.3668287

21. J. Zhang, Z. Li, J. Cao, M. Abdel-Aty, X. Meng, Global polynomial synchronization for quaternion-valued T–S fuzzy inertial neural networks via event-triggered control: a polynomial gain method, *Chaos Soliton. Fract.*, **196** (2025), 116403. https://doi.org/10.1016/j.chaos.2025.116403
22. X. Chen, D. Lin, Passivity analysis of non-autonomous discrete-time inertial neural networks with time-varying delays, *Neural Process. Lett.*, **51** (2020), 2929–2944. https://doi.org/10.1007/s11063-020-10235-6
23. Y. Wan, L. Zhou, Fixed-time synchronization of discontinuous proportional delay inertial neural networks with uncertain parameters, *Inf. Sci.*, **678** (2024), 120931. https://doi.org/10.1016/j.ins.2024.120931
24. Y. Chen, H. Liu, J. Hu, H. Lin, Dynamic event-triggered regional synchronization for discrete-time delayed dynamical networks: dealing with saturating actuators, *Neurocomputing*, **653** (2025), 131179. https://doi.org/10.1016/j.neucom.2025.131179
25. L. Yu, G. Chen, F. Jiang, Z. Wang, New criterias of synchronization for discrete-time recurrent neural networks with time-varying delay via event-triggered control, *Mathematics*, **10** (2022), 2816. https://doi.org/10.3390/math10152816
26. K. Udhayakumar, S. Shanmugasundaram, A. Kashkynbayev, R. Rakkiyappan, Saturated and asymmetric saturated control for projective synchronization of inertial neural networks with delays and discontinuous activations through matrix measure method, *ISA Trans.*, **142** (2023), 198–213. https://doi.org/10.1016/j.isatra.2023.07.022
27. W. Ma, X. Guo, H. Wang, Y. Zheng, Global inverse optimality for a class of recurrent neural networks with multiple proportional delays, *Inf. Sci.*, **662** (2024), 120240. https://doi.org/10.1016/j.ins.2024.120240
28. M. Iswarya, R. Raja, J. Cao, M. Niezabitowski, J. Alzabut, C. Maharajan, New results on exponential input-to-state stability analysis of memristor based complex-valued inertial neural networks with proportional and distributed delays, *Math. Comput. Simulat.*, **201** (2021), 440–461. https://doi.org/10.1016/j.matcom.2021.01.020
29. C. Aouiti, R. Sakthivel, F. Touati, Global dissipativity of fuzzy cellular neural networks with inertial term and proportional delays, *Int. J. Syst. Sci.*, **51** (2020), 1392–1405. https://doi.org/10.1080/00207721.2020.1764128
30. L. Li, W. Chen, Exponential stability analysis of quaternion-valued neural networks with proportional delays and linear threshold neurons: continuous-time and discrete-time cases, *Neurocomputing*, **381** (2020), 152–166. https://doi.org/10.1016/j.neucom.2019.09.051